Numerical analysis of stereolithography processes using the finite element method

Gabriel Bugeda, Miguel Cervera, Guillermo Lombera and Eugenio Oñate

The authors

Gabriel Bugeda, Miguel Cervera and **Eugenio Oñate** are all based in the Civil Engineering Department of the Technical University of Catalonia, Barcelona, Spain. **Guillermo Lombera** is based in the National Institute of Materials Technology, National University of Mar del Plata, Mar del Plata, Argentina.

Abstract

Stereolithography (SLA) is one of the most important techniques used in rapid prototyping processes. It has a great industrial interest because it allows for dramatic time savings with respect to traditional manufacturing processes. One of the main sources of error in the final dimensions of the prototype is the curl distortion effect owing to the shrinkage of the resin during the SLA process. Presents a study of the influence of different constructive and numerical parameters in the curl distortion, an analysis which was made using the computer code stereolithography analysis program, developed to model SLA processes using the finite element method. Also briefly presents this code.

Rapid Prototyping Journal
Volume 1 · Number 2 · 1995 · pp. 13–23
 · ISSN 1355-2546

Introduction

Most of the rapid prototyping processes are based on the manufacture of a given part starting from its computer-aided design (CAD) representation[1]. In the case of stereolithography (SLA) processes, the geometrical information is used to control the movement of a laser beam directed on to a radiation-curable resin photopolymer, producing its solidification. The final product depends on parameters like the type of resin, the laser power and the speed of its movement.

The SLA process can be summarized as follows. The liquid resin is placed into a recipient with a mobile platform. This platform is maintained at a fixed distance from the free surface of the resin. The movement of a laser beam is controlled using a system of galvanometers that move a mirror. When the laser beam illuminates the resin it produces its curing (solidification). The trajectory of the laser beam is controlled by a computer that contains the CAD geometrical information for the part to be built. Normally, the part geometry is defined using the 3D Systems' stereolithography (STL) format, which represents a surface triangulation. The volume of the part is sliced into different plane sections which provide the geometry of each one of the layers to be solidified by the laser beam. After the solidification of a layer, the platform descends so that the previously produced part is covered by the liquid resin that will provide the next layer. This process is repeated for each layer until the final part is produced[2].

After the SLA building process, the part is removed from the recipient and postcured for the solidification of the remaining liquid resin. After the postcuring process, the part is separated from the platform.

The main reason for the discrepancies between the CAD geometrical definition of the part geometry and the final part actually produced is the phenomenon known as "curl

This work has been performed in the context of the BRITE/EURAM project "Development of rapid prototyping technologies based on laser sintering", Contract no. BRE2-CT92-0228, Project no. BR-5478. The first author acknowledges the National Council of Scientific and Technical Investigations of the Republic of Argentina (CONICET) for its support of his stage at the International Centre of Numerical Methods in Engineering (CIMNE) in Barcelona through an external grant.

distortion''. This distortion is due to the shrinkage of the resin when it solidifies. The solidification of each layer produces the flexure of the layers solidified previously, as can be seen in Figure 1.

In addition, the postcuring process produces an additional tendency to shrink the remaining liquid resin. This tendency to shrink has been considered as uniform over the whole part for purposes of simplification.

When the part is separated from the platform, additional distortions can occur owing to the liberation of the internal forces that have developed between the part and the platform during the process.

The next sections will describe the development and implementation of a finite element model of the SLA process. This model has been used to predict the distortions corresponding to different part geometries. The comparison between the predicted and experimental values is presented for a set of examples.

Finite element model

In this section the finite element formulation for the equilibrium problem involved in SLA processes is described. This problem involves the solution of a standard set of second-order linear elliptic equations[3,4] in terms of the displacements u with appropriate boundary conditions:

$$Lu \equiv S^T DSu = v \text{ in } \Omega \qquad (1)$$

where u is the displacement vector at each point, v is the volumetric force, L is the second-order equilibrium differential operator, S is a first-order operator that provides the strains ε in terms of the displacements ($\varepsilon = Su$), and D is a matrix containing the elastic constants of the material.

In this work it has been assumed that the structural behaviour of SLA resins can be modelled using a linear elastic model with constant Young modulus and Poisson ratio. Clearly, this is an approximation because the resin behaviour during the SLA process is inelastic and the material properties do not remain constant. One of the objectives of this work is to check how feasible this approximation is.

Discretization of equation (1) using standard trial functions N for the approximation of the displacements ($u \approx \sum Na$) leads to the standard linear system of equations[3,4]:

$$Ka = f_\varepsilon \text{ with } \begin{cases} K = \sum_e K^{(e)} \\ K^{(e)} = \int_\Omega{}^{(e)} B^T DB d\Omega \\ f_\varepsilon = \sum_e f_\varepsilon^{(e)} \\ f_\varepsilon^{(e)} = \int_\Omega{}^{(e)} B^T D\varepsilon^0 d\Omega \end{cases} \qquad (2)$$

where K, a and f_ε denote the stiffness matrix, the nodal displacements and the equivalent nodal force vector caused by volumetric strains. Only gravity body forces are neglected in the analysis. Matrix $B = SN$ is used to obtain the strains at each point in terms of the nodal displacements as $\varepsilon = Ba$, and the constitutive matrix D relates strains to stresses as $\sigma = D\varepsilon$. The superscript $^{(e)}$ relates to a single finite element. The vector ε^0 contains the volumetric shrinkage of the resin:

$\varepsilon^0 = [\varepsilon^0, \varepsilon^0, 0]^T$ (for two-dimensional problems);

$\varepsilon^0 = [\varepsilon^0, \varepsilon^0, \varepsilon^0, 0, 0, 0]^T$ (for three-dimensional problems).

Linear and quadratic elements have been used for the solution of equation (1). Linear elements do not produce good solutions when parts are subjected to bending deformation. On the other hand, the use of quadratic elements is much more expensive than that of

Figure 1 Schematic side view of part building leading to curl distortion

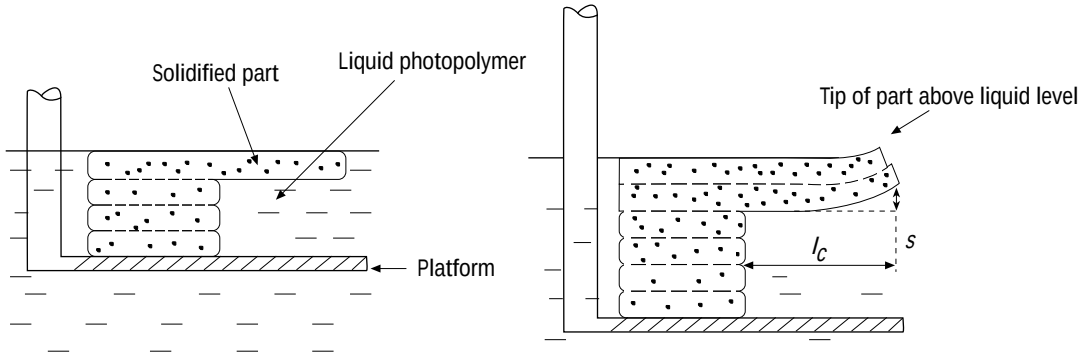

Rapid Prototyping Journal
Volume 1 · Number 2 · 1995 · 13–23

linear elements. In order to improve the behaviour of linear elements, a selective integration scheme has been used. This technique consists of the subintegration of the part of the stiffness matrix that corresponds to shear terms. For each element (e) its stiffness matrix $K^{(e)}$ is decomposed in two parts. The first one, $K_v^{(e)}$, contains the volumetric terms, and the second one, $K_t^{(e)}$, contains the shear terms:

$$K^{(e)} = K_v^{(e)} + K_t^{(e)} \tag{3}$$

with

$$K^{(e)}_{v_{i,j}} = \int^{\Omega_{(e)}} B^T_{v_i} D_v B_{v_j} d\Omega;$$
$$K^{(e)}_{t_{i,j}} = \int^{\Omega_{(e)}} B^T_{t_i} D_t B_{t_j} d\Omega. \tag{4}$$

For the two-dimensional case, these expressions are particularized to:

$$B_{v_i} = \begin{bmatrix} \dfrac{\partial N_i}{\partial x} & 0 \\ 0 & \dfrac{\partial N_i}{\partial y} \end{bmatrix}; \quad B_{t_i} = \begin{bmatrix} \dfrac{\partial N_i}{\partial x} & \dfrac{\partial N_i}{\partial y} \end{bmatrix} \tag{5}$$

and

$$D_v = \begin{bmatrix} d_{11} & d_{12} \\ d_{21} & d_{22} \end{bmatrix}; \quad D_t = \begin{bmatrix} d_{33} \end{bmatrix} \tag{6}$$

and for the plane stresses case:

$$d_{11} = d_{22} = \frac{E}{1-\nu^2}$$
$$d_{12} = d_{21} = \nu d_{11} \tag{7}$$
$$d_{33} = \frac{E}{2(1+\nu)} = G$$

where E and ν are Young's modulus and Poisson's ratio respectively.

Matrix K_v is computed using a second-order integration scheme whereas matrix K_t is computed using a first-order integration scheme.

Computational implementation

The finite element model described in the previous section has been implemented in the stereolithography analysis program (SLAP) code. This contains the necessary tools for the analysis of the SLA part-building process, the postcuring process and the final distortions produced when the part is separated from the platform. SLAP allows solution of two- and three-dimensional problems using four noded bilinear and eight noded quadratic quadrilateral elements in 2D and the corresponding eight and 20 noded cubiform elements in 3D.

A finite element mesh is generated starting from the CAD definition of the part geometry and producing a layer of elements corresponding to each layer of the SLA process. A new equilibrium problem is solved after the addition of each new layer over a previously built part. It is assumed that each new layer shrinks during its solidification, producing bending deformation of the previous part. After the solution of each equilibrium problem the geometry is actualized, adding the displacements produced by the shrinkage of the last layer. Figure 2 shows the step corresponding to the addition of the third layer after the actualization of the geometry of the first two layers. It is important to note that the upper surface of each new layer is always horizontal.

Depending on the volumetric shrinkage of the resin it is possible that the vertical displacements of the part produce the situation shown in Figure 3. In this case, Figure 4 shows how very thin elements are added in the zones of the part that rise over the free surface of the liquid resin.

The effect of the postcuring process has been modelled by introducing an additional uniform tendency to shrink the whole part after the building process. To introduce this additional tendency, a new nodal forces vector produced by a constant volumetric strain is added over the whole finite element mesh.

Figure 2 Construction of the third layer

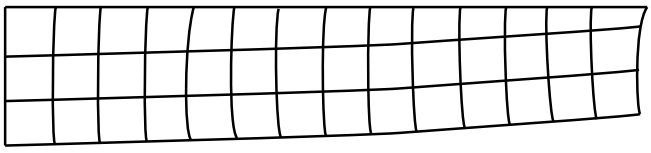

Figure 3 Distorted part over the free surface of the resin

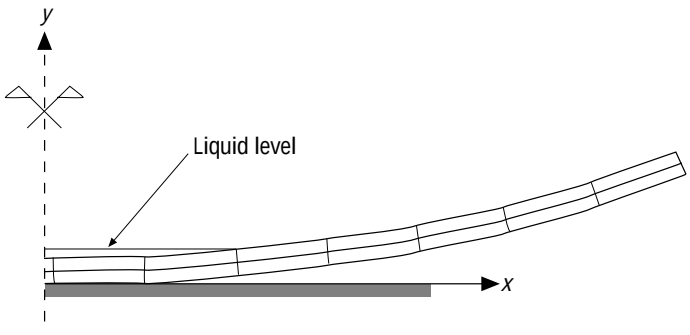

Figure 4 Construction of a new layer of elements for the case of parts rising over the free surface of the resin

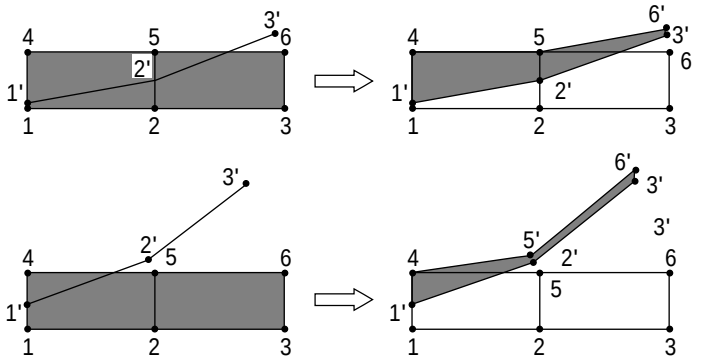

Figure 5 Twin cantilever geometry (in millimetres)

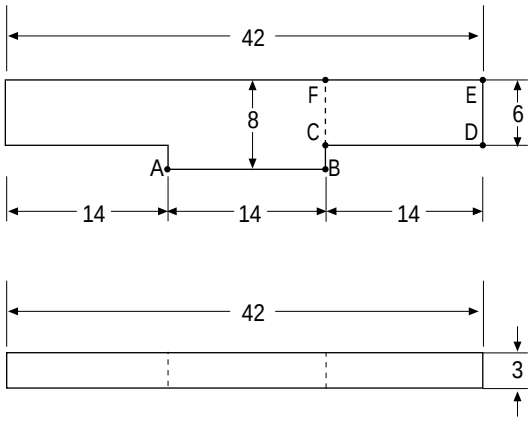

The part is attached to the platform by the interaction forces developed during the building and postcuring processes. These forces are liberated when the part and the platform are separated. During the finite element analysis of the building and postcuring processes, the values of these forces are obtained at the nodal points. In order to model the separation between the part and the platform, these forces are applied to the part with a negative sign.

Application examples

The SLAP code has been used for the analysis of different geometries and to study the influence of some parameters (layer thickness, volumetric shrinkage, Young's modulus and Poisson's ratio, etc.) in the distortions developed in parts produced by SLA processes. In the next sections the results corresponding to the analysis of some classical geometries are presented. These geometries correspond to a twin cantilever and the original stereolithography "user part".

Twin cantilever

The geometry of this case corresponds to one of the diagnostic testing examples described in Jacobs[2]. It is used to measure the influence of the volume shrinkage corresponding to some different resins in the final part distortions. The geometry of the twin cantilever is shown in Figure 5. This part is built using 24 layers 0.25mm thick.

This example has been analysed using 2D and 3D models, as well as different types of element, for comparison of all the possible strategies.

The cantilever curl distortion, C_{f6}, is defined as the curl elevation per unit length along the cantilever. It is measured at a 6mm unsupported cantilever length, and is expressed as a percentage:

$$C_{f6} = \frac{(M_6 - M_0)}{6\text{mm}} \times 100 = \frac{\Delta Z_6}{6\text{mm}} \times 100 \quad (8)$$

where M_6 is the elevation, in millimetres, of the bottom surface of the cantilever at an unsupported length of 6mm, and M_0 is the elevation, in millimetres, at the base of the cantilever. ΔZ_6 is the difference between these two values ($\Delta Z_6 = M_6 - M_0$). The choice of 6mm, somewhat arbitrary, was based on the observation that this value provides good measurement sensitivity and good repeatability without being subject to delamination effects.

Owing to the symmetry of the part, and taking into account that the base AB is totally fixed to the platform, only the part CDEF has been modelled in the first stage. A mesh with 14 elements along the cantilever length and 24 layers has been used. The final geometry for this case is shown in Figure 6.

Figure 7 shows a comparison between the results of the elevation of ΔZ obtained from the analysis and the experimental results taken from Jacobs[2].

Figure 6 Final geometry

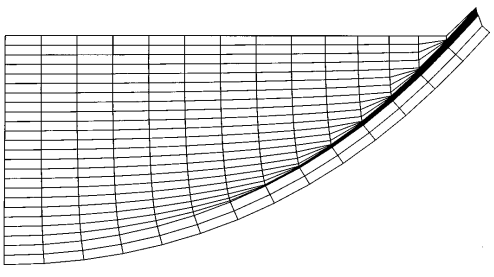

Rapid Prototyping Journal
Volume 1 · Number 2 · 1995 · 13–23

Figure 7 Comparison of results

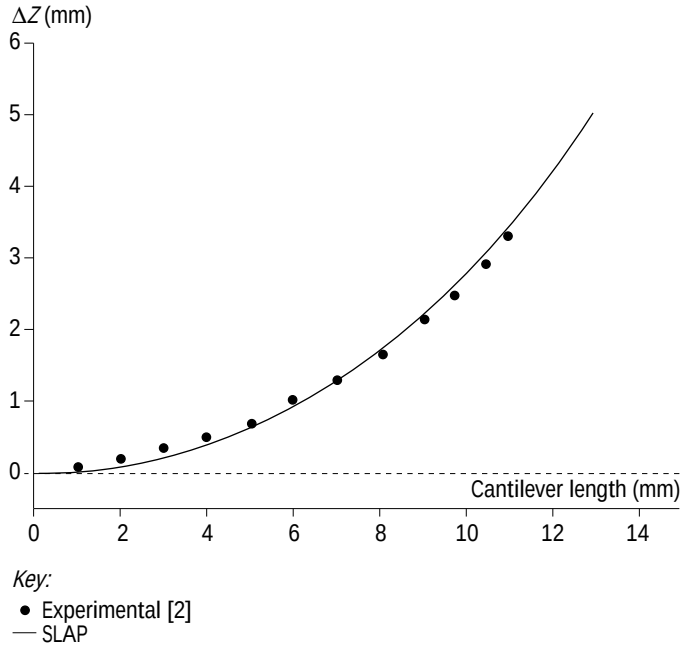

Figure 8 Constructive process for layers 3, 9, 18 and 24

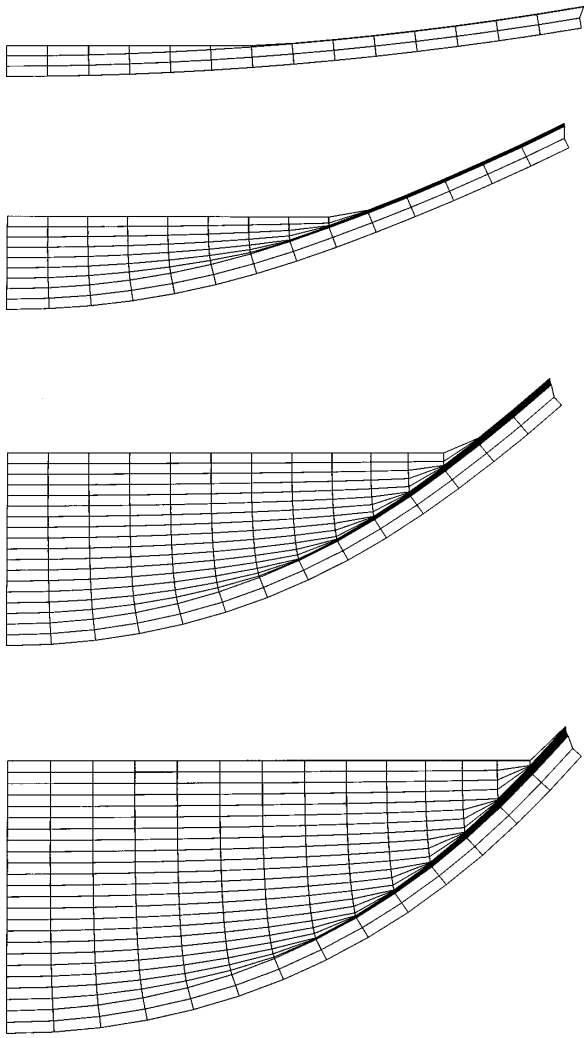

Influence of the volumetric shrinkage in the curl distortion

Figure 8 shows the geometries of the twin cantilever part corresponding to different stages of the part-building process. These results have been obtained using 2D eight-noded quadratic quadrilateral elements with full integration. The stages corresponding to the construction of layers 3, 9, 18 and 24 are represented.

Figure 9 shows the variation of the elevation ΔZ along the span of the cantilever. This variation is represented for different values of the volumetric shrinkage ε^0. It can be observed how the values of ΔZ, and the corresponding cantilever curl distortion, grow with the volumetric shrinkage.

Figure 10 shows the variation of ΔZ_6 with the magnitude of the volumetric shrinkage. It can be observed that this relationship is almost linear. On the other hand, Figure 11 shows the relation of the elevation ΔZ measured at different distances from the fixed point with the volumetric shrinkage. As it can be observed, the relationship for elevations measured at distances larger than 6mm is no longer linear. This is a justification for the measurement of the cantilever curl distortion at 6mm and not at a larger distance.

Influence of the layer thickness in the curl distortion

The cantilever of Figure 5 has been analysed using different layer thicknesses and four

Figure 9 Variation of the elevation with the volumetric shrinkage

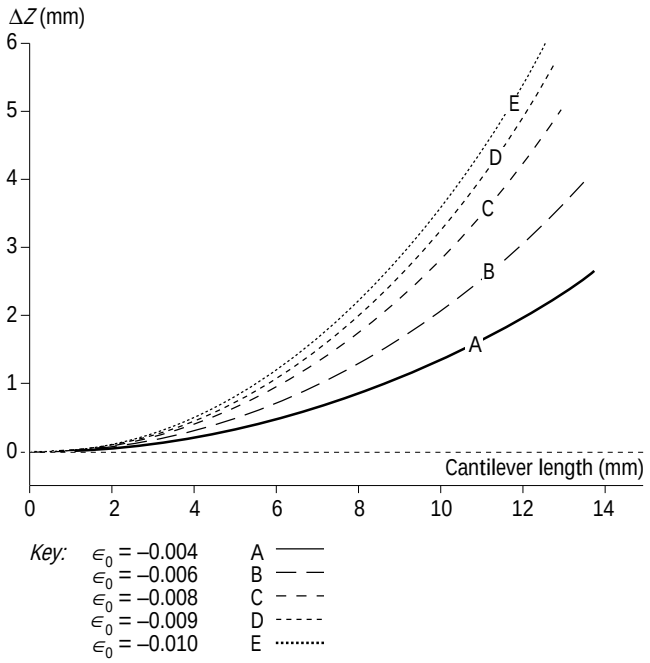

Rapid Prototyping Journal
Volume 1 · Number 2 · 1995 · 13–23

Figure 10 Variation of the elevation measured at 6mm. ΔZ_6 with the volumetric shrinkage

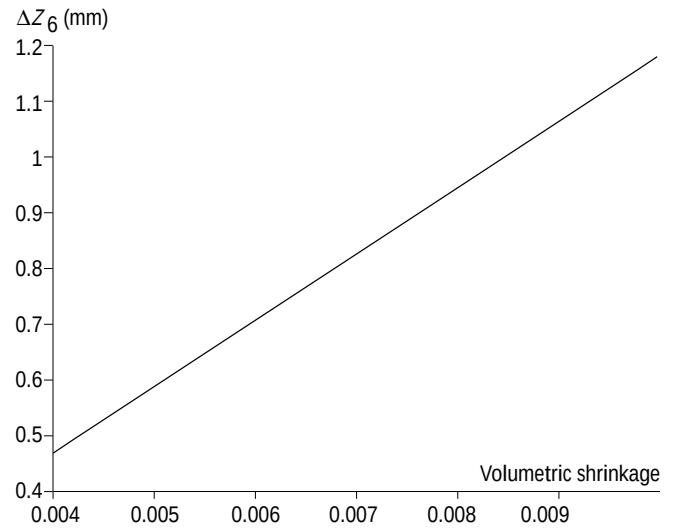

Figure 11 Variation of the elevation ΔZ measured at different distances with the volumetric shrinkage

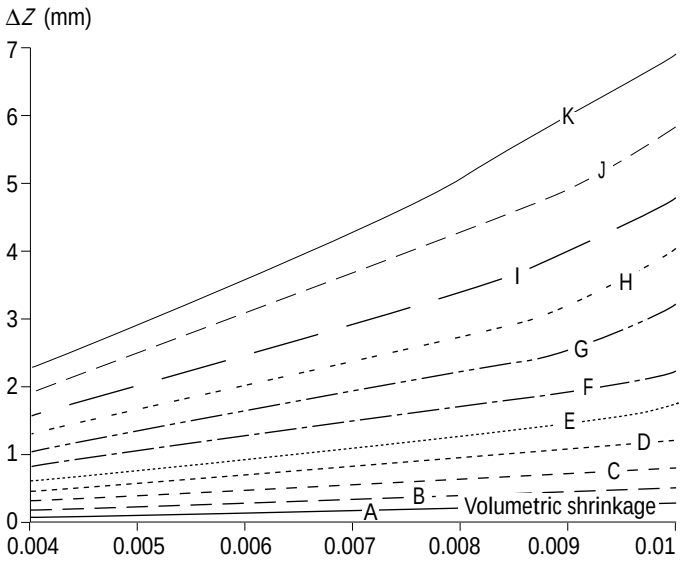

Figure 12 Final geometries obtained with 12 and 30 layers

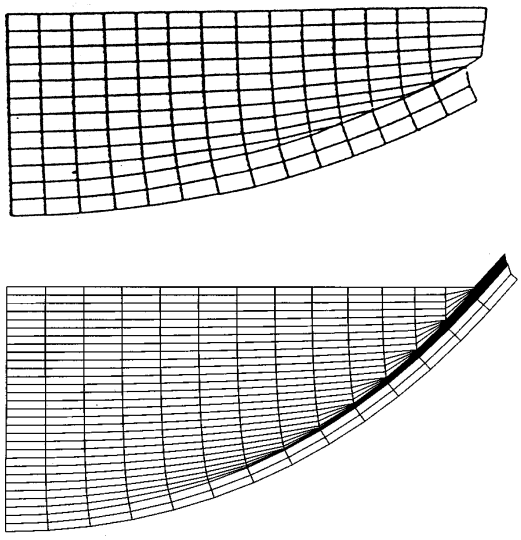

Figure 13 Variation of the elevation with the layer thickness

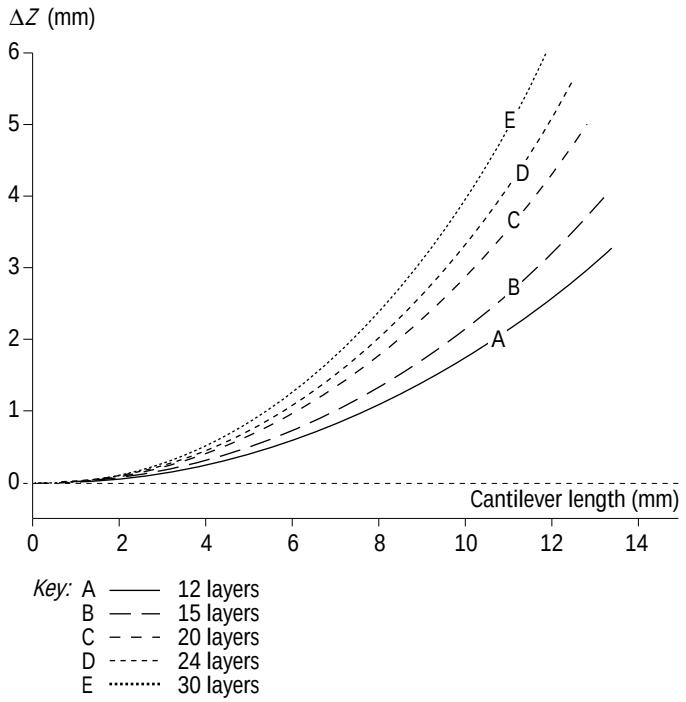

noded elements. The cantilever has been sliced into 6, 12, 15, 20, 24 and 30 layers. All the cases have been analysed using the same material parameters and with a volumetric shrinkage of $\varepsilon_o = 0.008$. Figure 12 shows the final geometries corresponding to the cases with 12 and 30 layers. Figure 13 shows the elevation ΔZ along the cantilever span corresponding to the different cases. Note how the curl distortion reduces when the layer thickness grows. This is in agreement with the conclusions of Jacobs[2].

Influence of the finite element mesh in the curl distortion

In order to evaluate the behaviour of the fully integrated four noded bilinear quadrilateral elements, the analysis of the cantilever has been repeated using different meshes. The cantilever span has been subdivided into 7, 14, 28, and 56 elements in order to see the evolution of the solution with an increasing

number of elements. Figure 14 shows the three first layers of the process corresponding to the cases with 7, 14, 28 and 56 subdivisions.

Table I shows a comparison between the horizontal and vertical displacements obtained for the points A, B and C of Figure 14 after the first two layers and for different meshes. These values are compared with the values obtained from the analytical solution obtained for the first two layers.

Figure 15 shows the variation of the elevation at each point obtained for each mesh. It can be observed how the solution improves with the number of elements but it is still too stiff, even for the finest mesh. This is because of the well-known bad behaviour of the four noded elements with full integration.

Figure 14 Deformed geometries corresponding to different meshes

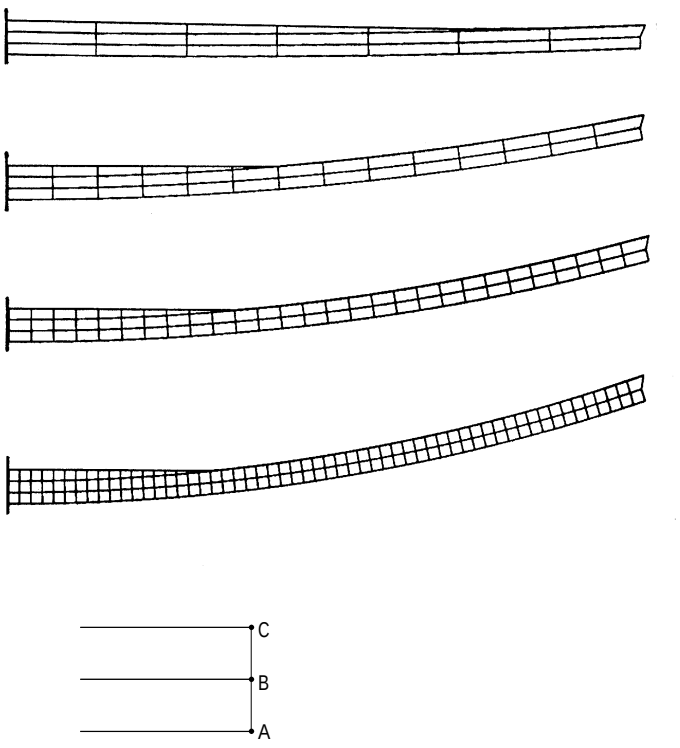

Figure 15 Elevations corresponding to different meshes. Definition of points A, B and C at the end of the cantilever

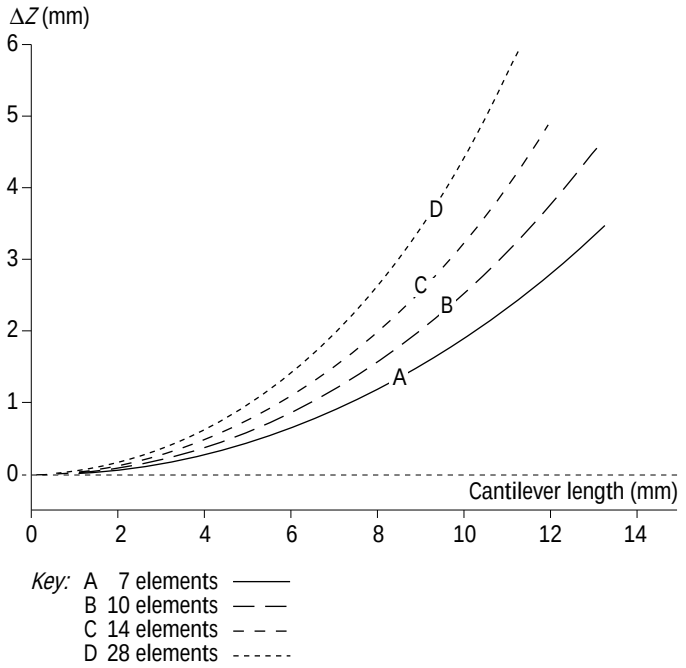

Comparison between different types of elements

Eight noded quadratic quadrilateral elements can reproduce analytical values with a low density of elements. Nevertheless, the cost of using eight noded elements is much higher than using four noded elements. This extra cost can be unacceptable for complex geometries where more than 1,000 layers may be needed.

Selective integration provides a tool to improve the behaviour of the four noded elements without increasing the computational cost. Table II shows a comparison between the displacements obtained with four noded elements with selective integration, eight noded elements and the analytical solution for two layers. For this case a mesh of 28 elements along the cantilever length has been chosen. It can be observed how selective integration improves the behaviour of the four noded elements.

Table I Horizontal (H) and vertical (V) displacements for points A, B and C using four noded quadrilateral elements compared with the analytical solution

Node	Displacements	7 elements	14 elements	28 elements	56 elements	Analytical solution
A	H	−0.0232	0.0033	0.0185	0.0236	0.0280
A	V	0.4556	0.8256	1.0357	1.1063	1.1760
B	H	−0.0556	−0.0555	−0.0555	−0.0556	−0.0560
B	V	0.4560	0.8259	1.0359	1.1064	1.1760
C	H	−0.0890	−0.1158	−0.1311	−0.1338	−0.1400
C	V	0.4587	0.8346	1.0481	1.1193	1.1760

Table II Horizontal (H) and vertical (V) displacements for points A, B and C using four noded bilinear quadrilateral elements with selective integration, and eight noded quadratic elements compared with the analytical solution

Node	Displacements	Four nodes with selective integration	Eight nodes	Analytical solution
A	H	0.0254	0.0267	0.0280
A	V	1.1316	1.1587	1.1760
B	H	−0.0554	−0.0554	−0.0560
B	V	1.1318	1.1595	1.1760
C	H	−0.1381	−0.1384	−0.1400
C	V	1.1456	1.1546	1.1760

Three-dimensonal analysis

For the three-dimensional analysis of SLA parts, the SLAP code allows use of cubiform linear (eight noded) as well as quadratic (20 noded) elements. These elements have similar characteristics to the corresponding two-dimentional ones. The eight noded elements with full integration have a very poor behaviour for bending deformation. The 20 noded elements have a much better behaviour but its computational cost cannot be accepted for large meshes. The eight noded elements with selective integration are a very good compromise between accuracy and computational cost.

Figure 16 shows the deformed geometries for the 3D analysis of the twin cantilever case after the construction of 6, 12, 18 and 24 layers.

Twin cantilever defined for the BRITE/EURAM 5478 project

In the context of the BRITE/EURAM Project no. 5478, "Development of rapid prototyping technologies based on laser sintering", a slightly different twin cantilever geometry has been used for comparison between the distortions obtained numerically and the experimental ones. The geometry used in this project is schematized in Figure 17. There are three different geometries corresponding to three different thicknesses of the cantilever. Each geometry has been built in six different positions in the SLA platform to avoid possible dependencies of the building process with respect to its orientation and position in the platform. Figure 18 shows a superposition of the initial and the final geometries corresponding to the case which is 2mm thick. The layer thickness for this example is 0.2mm and the volumetric shrinkage is $\varepsilon_o = 0.003$.

These geometries have been used for the calibration of the volumetric shrinkage ε_o used by the numerical model. The following steps have been followed for obtaining ε_o:

Figure 16 Deformed geometries corresponding to 6, 12, 18 and 24 layers using 3D eight noded cubiform elements with selective integration

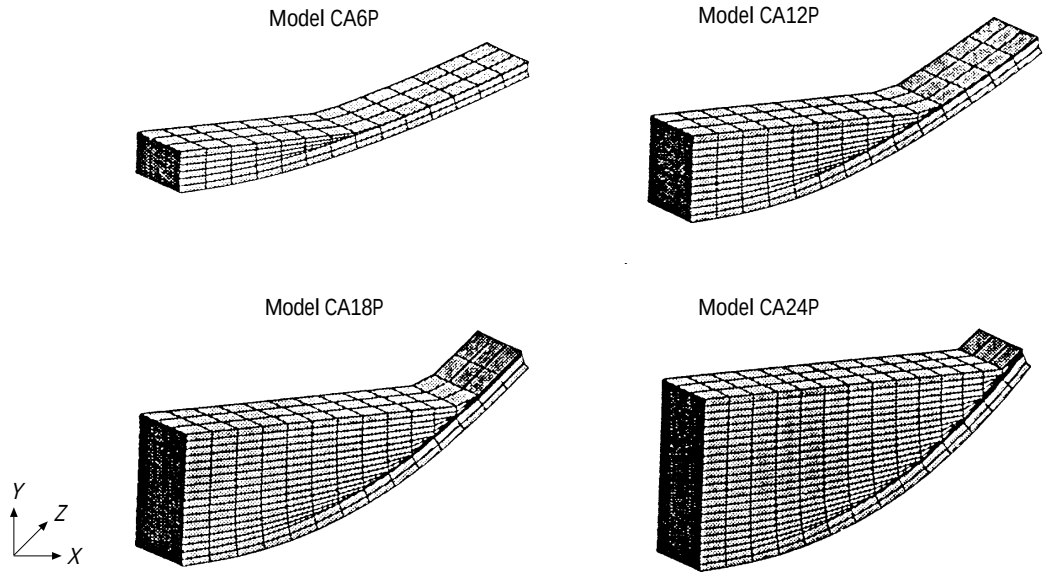

Figure 17 Geometry of the twin cantilever beam for the BRITE/EURAM project (in millimetres)

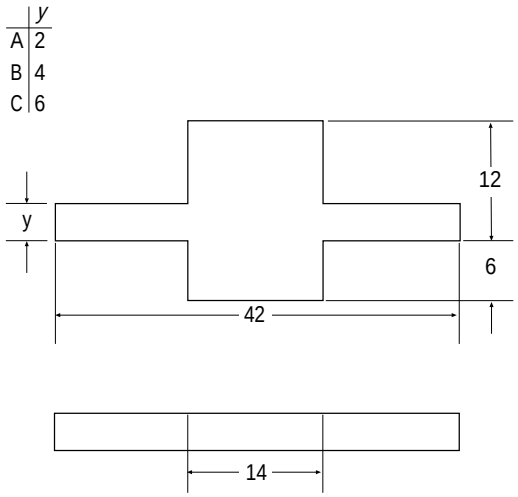

- For each one of the three different geometries, six different parts have been built using different positions and orientations in the platform. These are named BEAM 1, 2, 3, etc., in Figure 19.
- Before the postcuring process, the vertical displacements along each cantilever have been measured providing a "vertical displacements versus length" plot for each part.
- Using a least squares method, a single "vertical displacements versus length" plot has been fitted through all the parts' values.
- The part-building process of each geometry has been analysed with the finite element code using different volumetric shrinkages (0.001, 0.002, 0.003, 0.004, 0.005, 0.006, 0.007 and 0.008).

Figure 18 Initial and final geometries for y = 2mm

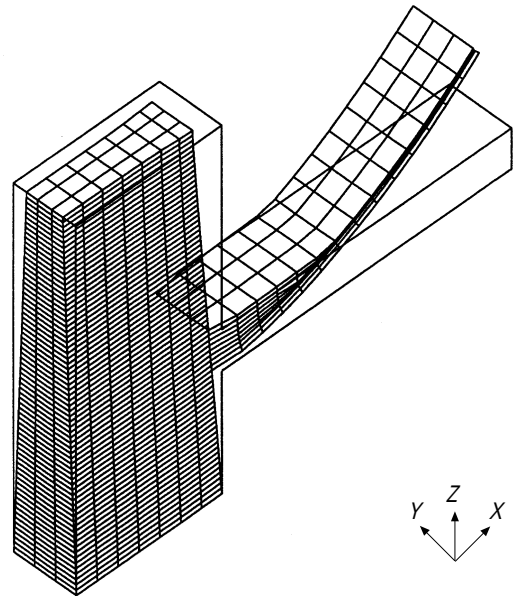

- For each of the used volumetric shrinkages, an index of the difference between the numeric and the experimental displacements has been computed. This index is computed as the sum of the squares of the differences between the numeric and experimental vertical displacements obtained at the measurements points. This measures the quality of the solution obtained with each volumetric shrinkage.
- A "quality index versus volumetric shrinkage" plot is interpolated using a least squares smoothing between the indexes corresponding to all the volumetric shrinkages. The minimum of this curve provides the volumetric shrinkage giving the numerical solution closest to the experimental one.

Figure 20 shows the curves corresponding to each of the three different geometries. For the curve corresponding to a geometry, the volumetric shrinkage corresponding to the minimum of the curve provides the best numerical solution. The three minima corresponding to the three geometries are very close and their mean value (ε_0 = 0.0027) has been chosen as that giving the best global adjustment for all the cases. Figure 19 shows the superposition

Figure 19 Superposition of the vertical displacements obtained with ε_0 = 0.0027 and the experimental values for the case which is 2mm cantilever thickness

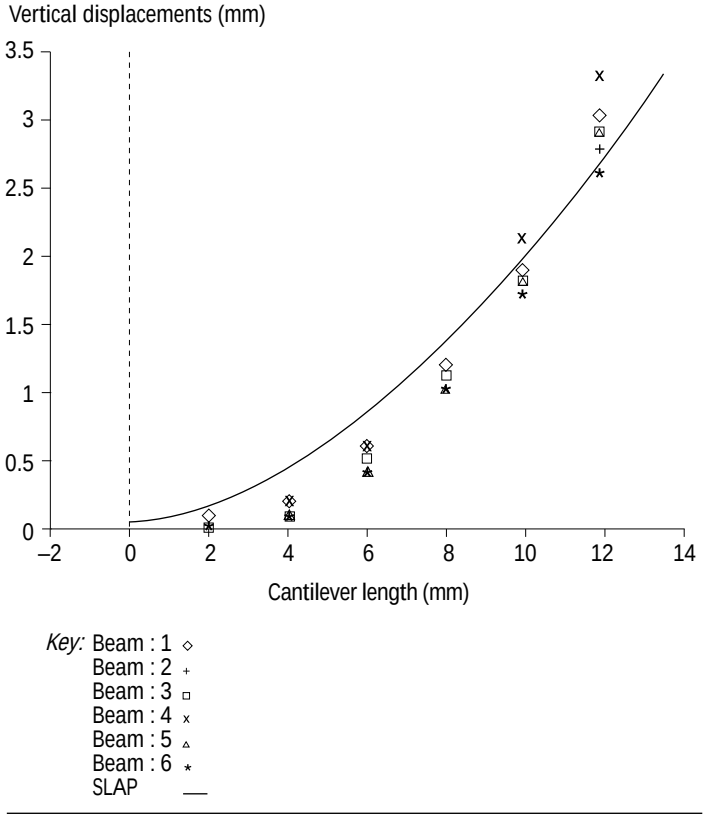

Figure 20 Least square adjustment of the quality index for each geometry (*H* = cantilever thickness)

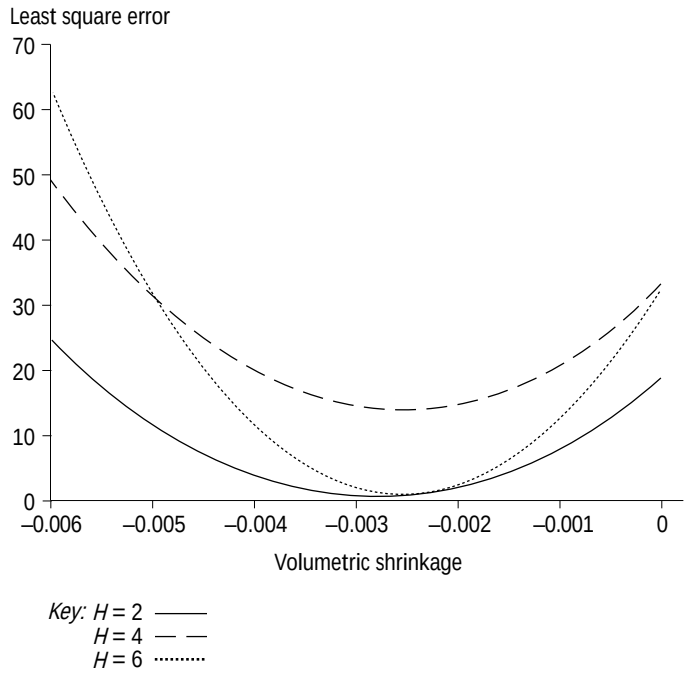

of the vertical displacements curve obtained with $\varepsilon_0 = 0.0027$ and the experimental values obtained for the six parts corresponding to the case which is 2mm thick.

The $\varepsilon_0 = 0.0027$ value will also be used for the numerical analysis of other geometries using the same SLA parameters.

Stereolithography user part

In this example, a more realistic three-dimensional geometry named "user part" has been chosen. This geometry was originally proposed in the USA by the Stereolithography Users Group and subsequently adopted as a reference standard for comparison between different rapid prototyping technologies. Figure 21 shows the CAD definition of the user part using a triangulation of its surface provided by the STL format.

The analysis of the user part has been performed using eight noded cubiform elements with selective integration. It has been assumed that the building process of the user part is controlled using the same parameters as in the previous twin cantilever case. Three different stages of the process have been taken into account:

(1) the SLA building process (a volumetric shrinkage $\varepsilon_0 = 0.0027$ obtained from the twin cantilever geometries has been used);

Figure 21 CAD definition of the user part

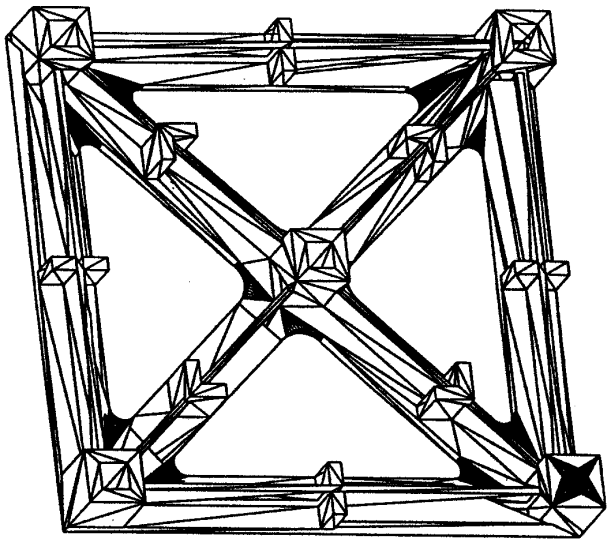

(2) the postcuring process (a volumetric shrinkage $\varepsilon_0 = 0.006$ has been chosen);
(3) the separation of the user part from the platform.

Figure 22 shows the superposition between the user part geometry and the final geometry obtained after the above mentioned three stages.

A comparison of this numerical solution with experimental measurements is expected to be reported soon.

Conclusions

A finite element model for the analysis of the part distortions during the SLA processes has been developed. This model has been implemented and tested into the SLAP code developed by the authors. Two- and three-dimensional cases have been analysed with a good agreement with experimental results. From the results of the different analyses performed with SLAP the following conclusions about the influence of different parameters in the final results can be drawn:

- The curl distortion grows with the magnitude of the volumetric shrinkage. The dependence of the curl distortion with respect to the magnitude of the volumetric shrinkage is linear only for short parts (less than 6mm). For longer parts it becomes non-linear.
- The curl distortion decreases when the layer thickness increases
- The four noded quadrilateral elements in 2D and the eight noded cubiform elements

Figure 22 Superposition between the initial and final geometry

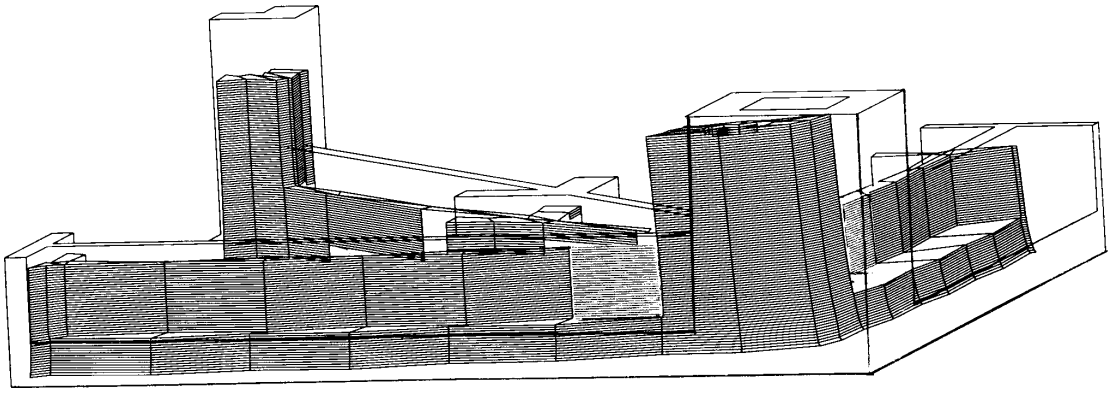

in 3D, both using selective integration, provide good results for the finite element analysis of SLA processes with an admissible computational effort.

References

1 Shellabear, M.C., Langer, H.J. and Cabrera, M., "The EOS rapid prototyping system", in Dickens, P.M. (Ed.), *Proceedings of the 1st European Conference on Rapid Prototyping,* University of Nottingham, Nottingham, 1992, pp. 19-26.

2 Jacobs, P., *Rapid Prototyping and Manufacturing Fundamentals of Stereolithography,* 1st ed., Society of Manufacturing Engineers, Dearborn, MI, 1992.

3 Zienkiewicz, O.C. and Taylor, R.L., *The Finite Element Method,* Vols I and II, McGraw-Hill, New York, NY, 1989 and 1991.

4 Oñate, E., *Cálculo de Estructras por el Método de Elementos Finitos – Análisis Estático* (Analysis of Structures by the Finite Element Method – Statical Analysis), International Centre of Numerical Methods in Engineering, Barcelona, 1992.

Further reading

Lart, G., "Comparison of rapid prototyping system", in Dickens, P.M. (Ed.), *Proceedings of the 1st European Conference on Rapid Prototyping,* University of Nottingham, Nottingham, 1992, pp. 243-54.

Lombera, G., Bugeda, G., Cervera, M. and Oñate, E., *SLAP: Programa para Modelado Numérico de Procesos de Estereolitografía Utilizando el Método de los Elementos Finitos* (*Program for the Numerical Modelling of Stereolithographical Processes Using the Finite Element Method*), CIMNE Publication No. 47, International Centre of Numerical Methods in Engineering, Barcelona, 1994.